Development of Simultaneous Optical Imaging and Super-Resolution Ultrasound to Improve Microbubble Localization Accuracy

J. Brown, S. Kolas, K. Christensen-Jeffries, C. De Menezes, S. Harput, J. Zhu, G. Zhang, M-X. Tang, C. Dunsby, and R. J. Eckersley.

***Abstract*— Acoustic super-resolution (SR) has the potential to visualize microvasculature by localizing individual microbubble (MB) signals. Currently, all detected signals are processed and localized identically. However, the MB point spread function (PSF) is not independent of its surroundings. Despite accuracy on the order of microns being required, it is currently not possible to quantify error that may be introduced due to variation in the MB responses.**

This work combines high frame rate plane wave ultrasound acquisition with a coincident optical microscope visualizing the SR imaging of a 200 µm cellulose tube. An adjustable aperture has been introduced into the optical microscope to extend the optical depth of field over the phantom.

The results showed that the introduction of the aperture enabled modest extension of the depth of field over 50 µm about the optical focus. Modelling and experimental verification found that, at a flow rate of 15 µl/min, MBs could only be detected over the top 70 µm of the tube phantom – further reducing the required depth of field. The simultaneous optical and acoustic data suggested that many fewer MBs acoustically contribute to the SR image than can be observed in the optical FOV.

Investigations incorporating a ground truth, like this one, will allow sources of error to be identified, quantified and limited.

I. Introduction

SUPER-RESOLUTION techniques which localize isolated microbubbles require an understanding of the relationship between microbubble response and position [1-6]. Previous authors have extracted isolated MB signals based on their signal strength and shape [6]. Once identified, the MB locations are determined using a general localisation technique, for example, centroiding [1] or Gaussian fitting [5]. It is well known that factors like MB size [7] nearby MBs [8] and boundaries [9] will affect the individual point spread functions. More work is required to determine how the environment of the MBs may affect their signal and thus the quality of super-resolution images.

A key challenge for acoustic super-resolution is validation of its accuracy and precision [10]. Previous work has used simulation to investigate this [11, 12], but experimental validation remains challenging. Previous authors have characterized the precision of SR by repeatedly localising a metal wire [1]. When imaging superficial structures, it can be possible to determine a ground truth using conventional microscopy [4]. Otherwise, in vivo, the improvement due to super-resolution techniques have widely been quantified by determining the full width half maximum (FWHM) of vessels [5, 13, 14]. However, none of these in vitro methods allow the contributions of individual MBs to the super-resolution image to be investigated. Without this ground-truth it is challenging to refine the SR technique.

There have been multiple optical studies of MB dynamics [9, 15-17], but none in the context of SR. These have generally involved isolation of MBs using either trapping techniques such as optical tweezers or by introducing a low concentration of MBs and imaging individual scatterers at rest on the phantom wall. For flowing microbubble distributions appropriate to super-resolution, the relative depths of field (DOF) of wide-field optical microscopy and ultrasound imaging make it challenging to match corresponding optical and acoustic data. The depth of field is the distance over which the object being imaged can be resolved. Thus, it is likely that a MB that appears isolated in the optical image will be affected by MBs visible in the larger acoustic FOV. Reducing the numerical aperture of a system can increase the DOF, but also reduce the resolution as shown by Equations 1 and 2:

This work was supported in part by the EPSRC under Grant EP/N015487/1 and Grant EP/N014855/1, in part by the King's College London and Imperial College London EPSRC Centre for Doctoral Training in Medical Imaging under Grant EP/L015226/1, in part by the Wellcome EPSRC Centre for Medical Engineering at King's College London under Grant WT 203148/Z/16/Z and in part by the Department of Health through the National Institute for Health Research Comprehensive Biomedical Research Center Award to Guy's and St Thomas' NHS Foundation Trust in partnership with the King's College London and King's College Hospital NHS Foundation Trust.

(Robert J. Eckersley, Christopher Dunsby, and Meng-Xing Tang contributed equally to this work.) (Corresponding author: Jemma Brown.)

J. Brown, S. Kolas, C. De Menezes, K. Christensen-Jeffries, and R. J. Eckersley are with the Department of Biomedical Engineering, School of Biomedical Engineering and Imaging Sciences, King's College London, London SE1 7EH, U.K. (e-mail: jemma.brown@kcl.ac.uk; samradnyee.kolas@kcl.ac.uk; cahil.de_menezes@kcl.ac.uk; kirsten.christensen- jeffries@kcl.ac.uk; robert.eckersley@kcl.ac.uk).

S. Harput, J. Zhu, G. Zhang, and M.-X. Tang are with the Ultrasound Laboratory for Imaging and Sensing Group, Department of Bioengineering, Imperial College London, London SW7 2AZ, U.K. (e-mail: s.harput@imperial.ac.uk; j.zhu16@imperial.ac.uk; ge.zhang15@imperial.ac.uk; mengxing.tang@imperial.ac.uk).

C. Dunsby is with the Department of Physics and the Centre for Pathology, Imperial College London, London SW7 2AZ, U.K. (e-mail: christopher.dunsby@imperial.ac.uk).

$$\Delta r = \frac{0.51\lambda}{NA} \quad (1)$$

$$DOF = \frac{n\cdot\lambda}{NA^2} + \frac{n\cdot e}{M\cdot NA} \quad (2)$$

Wavelength (λ)
Pixel size (e)
Magnification (M)
Refractive index of water (n)
Numerical Aperture (NA)

Water immersive objectives with suitable numerical apertures and magnifications are not commercially available. This work introduces the novel approach of using an adjustable optical aperture to extend the DOF. This system has the flexibility of reducing the numerical aperture without changing the magnification.

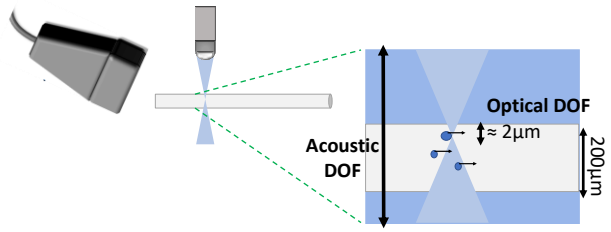

Fig 1. Comparing DOFs of plane wave US imaging and wide field optical microscopy.

After characterisation of the optical system, simultaneous optical and acoustic data were collected with the aim of determining how MB environment will affect the localisations.

II. METHODS

A. *In silico*

An adjustable aperture (Thorlabs) was inserted as close to the back aperture of a water immersion x40 microscope (LUMPLANFLN, Olympus) as permitted by the optomechanics used, and the image focused on a CMOS sensor (Ximea). The optical set-up is shown in Figure 2. The resolution over the DOF was characterized using a sector star resolution target (ThorLabs), where contrast between bright and dark bars provides a measure of resolution. The smallest resolution measurable was 115 lp/mm, corresponding to a modulation period of 8.6 µm. Contrast was calculated by measuring the intensity profile over arcs at 4 µm intervals as shown in Fig. 3 (A). The difference between the mean value of the maxima and minima of the profile is reported as the contrast in Fig. 3(B and C).

A 200 µm cellulose tube was chosen as a vessel phantom. A dilute Sonovue™ (Bracco) microbubble solution was drawn through the cellulose phantom at flow rates between 15-50 µl/min. Using the widest possible aperture, the MB flow was characterized at 10 µm increments across the extent of the tube to map the MB flow distribution. This was compared with theory by modelling the MB parabolic flow.

Optical data was collected before and after the triggering of plane wave ultrasound using an ULA-OP system (MSD Lab, University of Florence). A LA332 (Esaote) probe was operated at center frequency of 4 MHz, with contrast sequence (1,-1, ½) at a pulse repetition frequency of 400 Hz. The contrast images were processed using amplitude modulation to give a frame rate of 133 Hz. Pulse amplitude was chosen such that MBs were not significantly diminished by destruction over the acquisition. The camera was used at a frame rate of approximately 70 Hz.

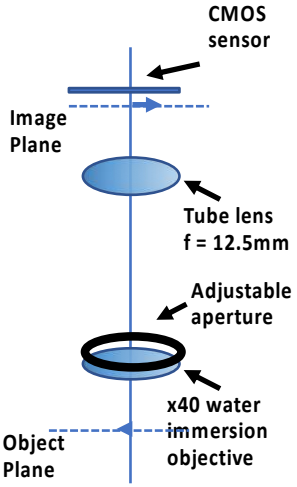

Fig 2: Ray diagram of optical set-up.

III. RESULTS

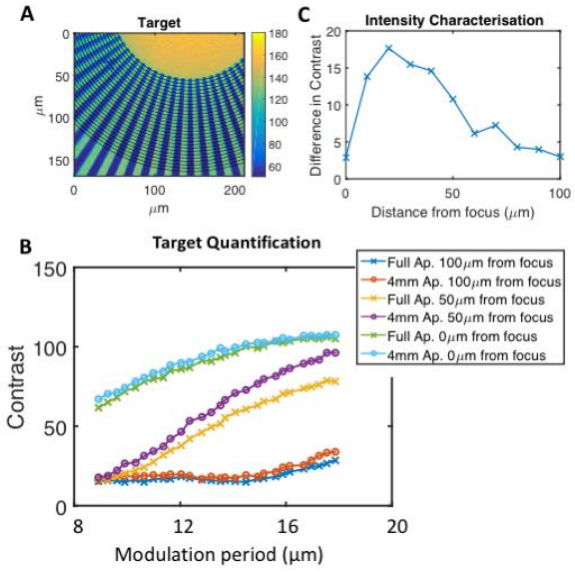

Fig 3: Characterisation of optical DOF and resolution. (A) Example image of optical target with profiles indicating where intensity profiles were calculated. (B) Plotting contrast over resolution at 100 µm, 50 µm and 0 µm from the focus for the full aperture and 4 mm aperture. (C) The average difference in contrast between the full aperture and 4mm aperture, calculated as an average over all periods of modulation measured and at 10 µm increments away from the focus is shown.

An aperture 4 mm in diameter was the smallest possible to avoid obscuring the image. Fig. 3 shows that the most improvement in contrast could be achieved over the range 10 - 50 µm from the optical focus. When optically detecting MBs, the current algorithm can detect MBs that have a difference in contrast of 27.2 units. Thus, an improvement of that shown in Fig. 3 should increase the number of MBs being detected over approximately 50 µm about the focus.

It was empirically observed that MBs could only be optically detected over the upper half of the tube. Modelling of the MB flow considering drag, gravity, buoyancy and parabolic flow showed that buoyancy would be expected to have a significant effect at low MB flow speeds. For example, after flowing a distance of 5 cm, Fig. 4 (A and B) show that a MB of radius 1 µm and maximum speed of 1 mm/s would only be expected to be found in the upper 50 µm of the tube. This was experimentally investigated using the full aperture and counting MBs at 10 µm intervals over the tube extent as shown in Fig. 4 (C). The experimental results suggest that MBs are most likely to be found in the upper 70 µm of the tube.

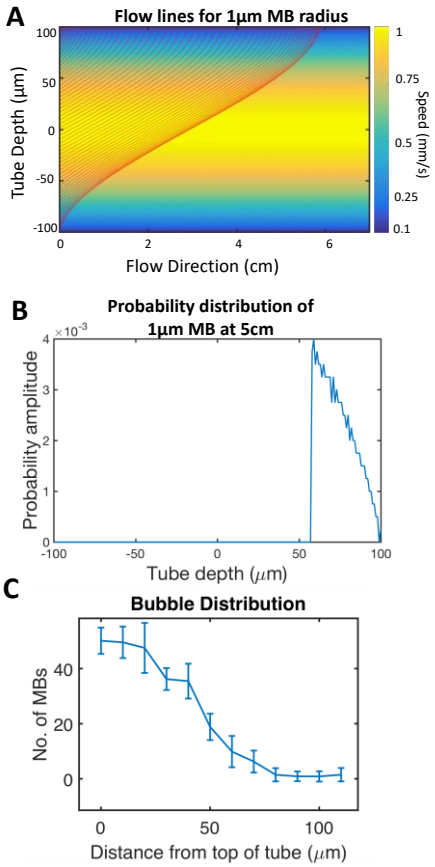

Fig 4: Characterisation of MB position over tube. (A) Modelled flow profiles of MB 1 µm in radius and (B) the probability of finding a MB over the tube extent, where a depth of 0 µm corresponds to the tube center. (C) Experimentally determined distribution of all MBs over tube extent.

Perhaps naively, it was expected that the majority of MBs would be acoustically active, such that only a few MBs would be observable in the optics for acoustic data suitable for SR. However, a typical example of simultaneous acoustic and optical acquisition is shown in Fig. 5. The acoustic frame can generate only 8-10 localisations over the entire FOV, however there are tens of MBs over a small portion of the phantom (< 200 µm in length).

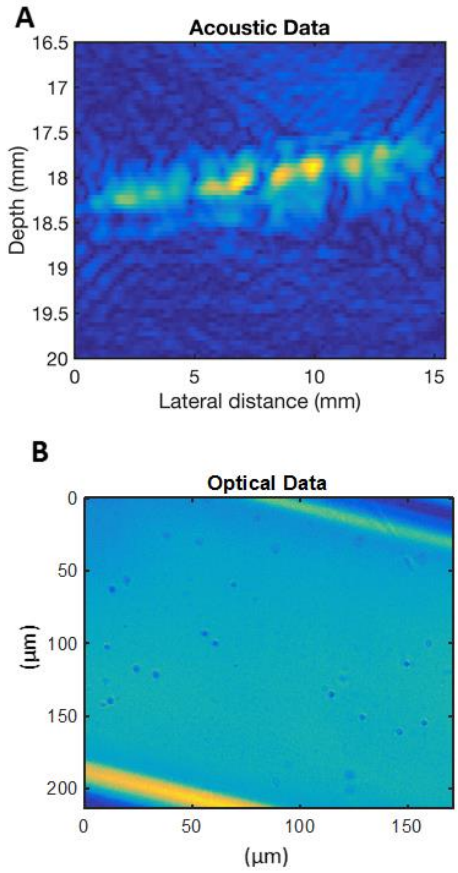

Fig 5: Simultaneous US and optical imaging (A) Example acoustic amplitude modulation frame for a tube phantom running parallel to the transducer surface (B) The corresponding optical frame imaging a cross-section of the tube, in the centre of the acoustic FOV, perpendicular to the direction of gravity. The optical and acoustic set ups are positioned at right angles to each other. Note the difference in scales between A and B.

V. Discussion

This work has shown that introduction of an adjustable aperture is a cheap and flexible way of increasing the likelihood of MB detection approximately 50 µm about the optical focus. In focus, we would expect the open aperture to be preferable for resolving the smallest objects. However, the optical target used for this characterization did contain high enough spatial frequencies for this to be measured.

At flow rates of a few millimeters per second, MBs are only observed in the upper portion of the tube due to buoyancy. This

further reduces the DOF necessary and informed where the optical focus of later experiments should be set.

Over the process of generating these results, it was found to be very challenging to achieve acoustic data that was suitable for SR at slow flows. It was easier to obtain acoustic data with strong isolated signals by increasing the flow rate to around 50 µl/min. This was because it was possible to use a higher pulse amplitude without destruction of the MBs. However, at faster flow, the optical set-up did not have a high enough frame rate to capture the flowing MBs. Thus, it was not possible to assess what fraction of MBs were contributing to the acoustic signals. SR imaging has already been demonstrated at low flow velocities (<1 mm/s) in vivo [4]. However, previous work has also shown problems with collecting appropriate data at slow flows using tube phantoms [18]. Previous literature has shown that tube size has an effect on MB behavior [19]. Future work will involve assessing whether the vessel phantom prohibitively affects the MB response and if a new flow phantom is required for more realistic in vitro studies.

It was unexpected that many more MBs would be detected in the optics for few isolated acoustic signals. If it is the case that only a small fraction of the MBs are useful for SR imaging, perhaps the injected MB distribution could be optimized to increase the proportion of useful scatterers. Future work will involve collecting data using very low concentrations over several hours to generate a library of corresponding optical and acoustic images.

VI. Conclusions

Overall this work has shown that the introduction of an adjustable aperture is a flexible and cheap method of increasing DOF without affecting system magnification. At flows on the order of a few mm/s, buoyancy further reduces the required DOF to <70 µm. A lower fraction of MBs contribute to the acoustic SR image than expected. Future work will determine which MB characteristics determine their contribution to the SR image.

VII. References

1. Viessmann, O., et al., *Acoustic super-resolution with ultrasound and microbubbles.* Physics in medicine and biology, 2013. **58**(18): p. 6447.
2. O'Reilly, M.A. and K. Hynynen, *A super-resolution ultrasound method for brain vascular mapping.* Medical physics, 2013. **40**(11): p. 110701.
3. Desailly, Y., et al., *Sono-activated ultrasound localization microscopy.* Applied Physics Letters, 2013. **103**(17): p. 174107.
4. Christensen-Jeffries, K., et al., *In vivo acoustic super-resolution and super-resolved velocity mapping using microbubbles.* Medical Imaging, IEEE Transactions on, 2015. **34**(2): p. 433-440.
5. Errico, C., et al., *Ultrafast ultrasound localization microscopy for deep super-resolution vascular imaging.* Nature, 2015. **527**(7579): p. 499-502.
6. Ackermann, D. and G. Schmitz, *Detection and Tracking of Multiple Microbubbles in Ultrasound B-Mode Images.* Ultrasonics, Ferroelectrics, and Frequency Control, IEEE Transactions on, 2016. **63**(1): p. 72-82.
7. Van der Meer, S., et al. *The resonance frequency of SonoVue™ as observed by high-speed optical imaging*. in *Ultrasonics Symposium, 2004 IEEE*. 2004. IEEE.
8. Crum, L.A., *Bjerknes forces on bubbles in a stationary sound field.* The Journal of the Acoustical Society of America, 1975. **57**(6): p. 1363-1370.
9. Vos, H.J., et al., *Nonspherical Vibrations of Microbubbles in Contact with a Wall-A Pilot Study at Low Mechanical Index.* Ultrasound in Medicine and Biology, 2008. **34**(4): p. 685-688.
10. Couture, O., et al., *Ultrasound Localization Microscopy and Super-Resolution: A State of the Art.* IEEE transactions on ultrasonics, ferroelectrics, and frequency control, 2018. **65**(8): p. 1304-1320.
11. Desailly, Y., et al., *Resolution limits of ultrafast ultrasound localization microscopy.* Physics in medicine and biology, 2015. **60**(22): p. 8723.
12. Brown, J., et al. *Investigation of microbubble detection methods for super-resolution imaging of microvasculature*. in *Ultrasonics Symposium (IUS), 2017 IEEE International*. 2017. IEEE.
13. Lin, F., et al., *3-D ultrasound localization microscopy for identifying microvascular morphology features of tumor angiogenesis at a resolution beyond the diffraction limit of conventional ultrasound.* Theranostics, 2017. **7**(1): p. 196.
14. Harput, S., et al., *Two-Stage Motion Correction for Super-Resolution Ultrasound Imaging in Human Lower Limb.* IEEE transactions on ultrasonics, ferroelectrics, and frequency control, 2018. **65**(5): p. 803-814.
15. Dayton, P.A., et al., *Optical and acoustical observations of the effects of ultrasound on contrast agents.* IEEE transactions on ultrasonics, ferroelectrics, and frequency control, 1999. **46**(1): p. 220-232.
16. Garbin, V., *Optical tweezers for the study of microbubble dynamics in ultrasound.* 2006.
17. Sijl, J., et al., *Combined optical and acoustical detection of single microbubble dynamics.* The Journal of the Acoustical Society of America, 2011. **130**(5): p. 3271-3281.
18. Christensen-Jeffries, K., *Super-resolution ultrasound imaging with microbubbles* in *Division of Imaging Sciences and Biomedical Engineering*. 2016, King's College London: London.
19. Caskey, C.F., et al., *Microbubble oscillation in tubes with diameters of 12, 25, and 195 microns.* Applied Physics Letters, 2006. **88**(3): p. 033902.